UDC 544.6:542.8

O.L. Riabokin [a], K.D. Pershina [a, b]

APPLIED ASPECTS OF USING ELECTROCHEMICAL IMPEDANCE SPECTROSCOPY SPECTRA FOR MONITORING ELECTRODE DAMAGE AND ELECTROLYTE DEPLETION IN PRIMARY ZINC-MANGANESE BATTERIES

[a] V.I. Vernadsky Institute of General and Inorganic Chemistry, National Academy of Sciences of Ukraine, Kyiv, Ukraine
[b] National Technical University of Ukraine «Igor Sikorsky Kyiv Polytechnic Institute», Kyiv, Ukraine

The article presents experimental and computational data on monitoring electrode surface condition and electrolyte depletion in primary Zn-Mn batteries using electrochemical impedance spectroscopy and scanning electron microscopy with backscattered electrons. These methods reveal the impact of different current load levels on changes in electrode surfaces and their chemical composition. Through comparative analysis of data from standard tests and electrochemical impedance spectroscopy spectra using mathematical tools for alternating current analysis, the feasibility of accurately assessing the operational state of primary batteries is demonstrated. The results obtained can be applied to studies of irreversible changes in chemical power sources and to the development of the theory of porous electrodes.

Keywords: zinc-manganese primary battery, non-Faradaic capacitance, capacity dispersion, electrode damage, electrolyte depletion.

DOI: 10.32434/0321-4095-2025-158-1-32-38

Introduction

Electrochemical impedance spectroscopy (EIS) is widely used to measure and study the interfacial and bulk electrochemical properties of materials and devices [1]. There are many methods that allow determining various electrochemical parameters using EIS [1–5]. The most well-known is the method of constructing equivalent electrochemical circuits with an appropriate set of elements that simulate the behavior of the components of the electrochemical system (electrodes, interphase interactions between the electrode and the electrolyte, ion diffusion, etc.). With regard to chemical current sources, the most informative is the construction of equivalent electrochemical circuits, which commonly include a Warburg element and a constant phase element. The presence of these elements, as a rule, indicates the emergence of diffusion-controlled processes in electrochemical systems [1–5] (solid-state electronic devices [6,7], solid-state ionites [8] and chemical current sources).

However, the electric energy is stored in capacitors, particularly in an electrochemical double layer (Helmholtz layer) formed at a solid/electrolyte interface. Positive and negative ionic charges within the electrolyte accumulate at the surface of the solid electrode and compensate for the electronic charge at the electrode surface. The thickness of the double layer depends on the concentration of the electrolyte and the size of the ions and is on the order of 5–10 Å for concentrated electrolytes. The double layer capacitance is about 10–20 $\mu F/cm^2$ for a smooth electrode in concentrated electrolyte solution and can be estimated according to equation Eq. (1) assuming a relative dielectric constant of 10 for water in the double layer [5].

$$C = \frac{\varepsilon_0 \varepsilon A}{d}, \quad (1)$$

where d is the thickness of the double-layer with surface area of A.

The corresponding electric field in the electrochemical double layer is very high and assumes values of up to 106 V/cm. Compared to conventional capacitors where a total capacitance of pF and μF is typical, the capacitance of and the energy density stored in the electrochemical double layer is rather high per se. To achieve a higher capacitance, the electrode surface area is additionally increased by using porous electrodes with an extremely large internal effective surface. The combination of two such electrodes gives an electrochemical capacitor of rather high capacitance.

Electrolytes have their specific resistance. The electrolyte resistance also affects the distributed resistance of the porous layer and consequently reduces the maximum usable power, which is calculated according to the following equation:

$$P = \frac{U^2}{4R}, \quad (2)$$

where R represents the total effective series resistance (ESR).

The presence of a porous structure activates the immobilization of the liquid electrolyte by capillary forces. In this case, the reduced free volume for the liquid electrolyte is expected a decrease conductivity, increase ohmic losses, and change the distribution of capacitance. The passivation and densification of the zinc electrode have been identified as the principal causes of the poor lifetime of the battery due to the formation of the dendrites in the direction of increasing zincate concentration [1,6].

This work is aimed to discuss the applied possibility of control the capacitance changes after current loads in primary Zn-Mn batteries by electrochemical impedance spectroscopy.

Experimental

Series (5 batteries per series) of primary alkaline Zn-Mn cells with a voltage of 1.5 V was discharged in galvanostatic mode by using a PI-50-1 potentiostat under a direct current density of 10, 20, 30, 40, 50, and 60 mA/cm^2 at a temperature of 20±5^{0}C for 80 minutes (Table 1).

Before starting the discharge, the samples were kept for 1.5±0.2 h to establish temperature equilibrium in the system. The value of the discharge currents was calculated based on the nominal capacity of the cells. The internal resistance at direct current was calculated according to the following equation:

$$R = \frac{U_s - U_f}{I_2 - I_1}, \quad (3)$$

Table 1

Electrical parameters of the tested primary batteries

Series of samples	Discharge current density, mA/cm^2	Ending voltage, V	Resistance, Ohm
1	10±1	1.55±0.05	9.37±0.05
2	20±1	1.51±0.05	8.37±0.05
3	30±1	1.47±0.05	6.12±0.05
4	40±1	1.43±0.05	5.92±0.05
5	50±1	1.39±0.05	5.66±0.05
6	60±1	1.38±0.05	5.08±0.05

where U_s is the starting voltage; U_f is the finishing voltage; I_2=0.2I_1; I_1 is the discharge current.

The test of internal resistance and state of batteries was carried out by using the Autolab-30 electrochemical module, PGSTAT301N Metrohm Autolab, equipped with the FRA (Frequency Response Analyzer) module in the frequency range of 10^{-2}—10^6 Hz, the amplitude of the disturbing signal being ±5 mV. The FRA module was controlled using the Autolab 4.9 program. Processing of the obtained results was carried out in the Zview 2.0 software.

Backscattered electron (BSE) images obtained by scanning electron microscopy (SEM) were used to control the changes on electrode surface (morphological and component).

Calculations of the capacitance from impedance spectra were done using the following impedance spectroscopy equations:

$$\theta = \tan^{-1}\left(\frac{X_C}{R}\right), \quad (4)$$

$$X_C = \frac{1}{\omega C}, \quad (5)$$

$$C = \frac{1}{\omega X_C}, \quad (6)$$

$$C_\omega = 1/[Z_\omega - Z_{\omega\to\infty}]i\omega, \quad (7)$$

$$Z = R + jX + |Z|\Delta\theta, \quad (8)$$

Results and discussion

Measurements of the electrical parameters of the primary battery after discharge showed that, with an increase in the current density above 30 mA/cm^2, the differences in the discharge galvanostatic curves and internal resistance values become insignificant (Table 1). Impedance spectra are more sensitive to changes in the current density of batteries (Fig. 1 and 2). The radius of the semicircles shows a monotonic decrease under current loads from 10 to

30 mA/cm^2 on the Nyquist plots; and they disappeared at more than 30 mA/cm^2. The shifts of phase angles have the same tendency (Fig. 3 and 4). In this case, not only absolute data of phase angle changes but also the maxima of phase angle shift to the low-frequency range.

Most electrochemical cells do not imply uniform current distribution through a definite electrolyte area. The major problem in controlling electrolyte depletion concerns the determination of the resistance of the current flow path and the geometry of the electrolyte that carries the electrical current. In the case of primary Zn-Mn battery, the appearance of zinc salts changes the density of the electrolyte and forms the conditions of the density and concentration gradient generation [9]. The zinc electrode compartment the electrode process consumes zincate ions and produces hydroxyl ions during charge; inversely, during discharge, it

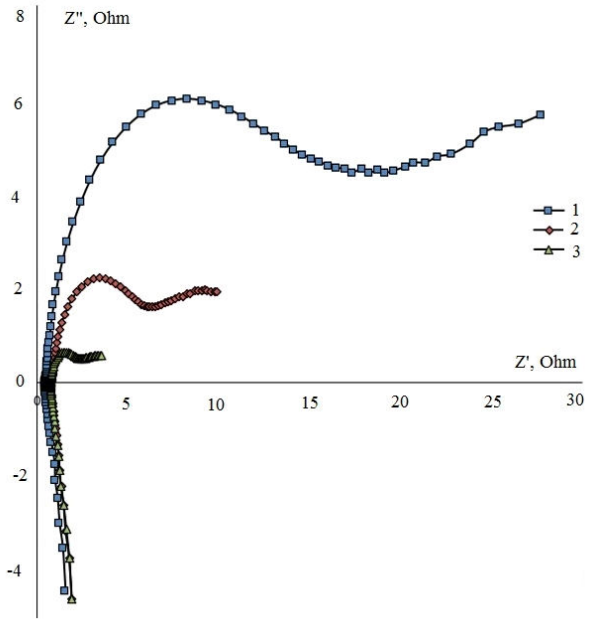

Fig. 1. Nyquist plots after different current loads: (1) 10 mA/cm^2; (2) 20 mA/cm^2; and (3) 30 mA/cm^2

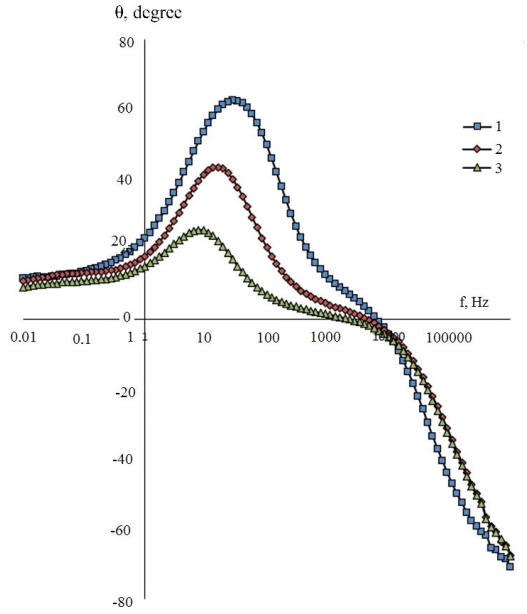

Fig. 3. Bode plots after different current loads: (1) 10 mA/cm^2; (2) 20 mA/cm^2; (3) 30 mA/cm^2

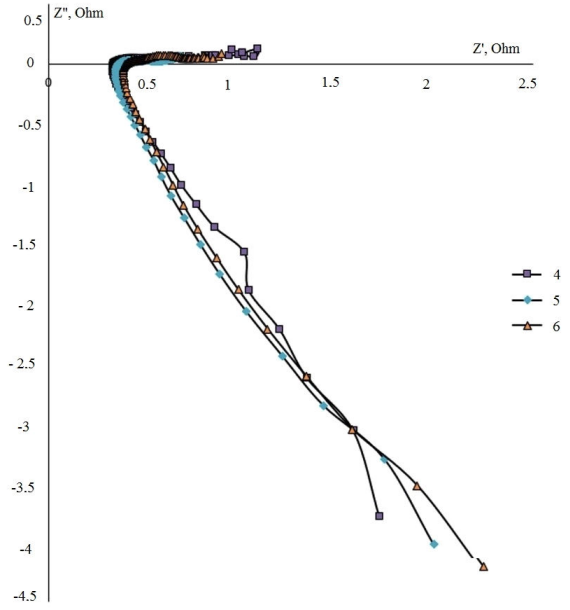

Fig. 2. Nyquist plots after different current loads: (4) 40 mA/cm^2; (5) 50 mA/cm^2; and (6) 60 mA/cm^2

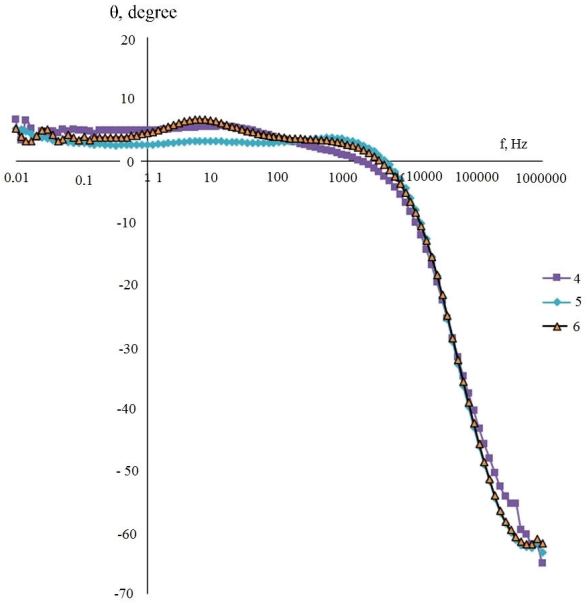

Fig. 4. Bode plots after different current loads: (4) 40 mA/cm^2; (5) 50 mA/cm^2; and (6) 60 mA/cm^2

produces zincate ions and consumes hydroxyl ions (density gradient model) [10]. This model is based on the study of zinc electrodes in alkaline media named B-mechanism [11]:

$$Zn+OH^- \rightarrow ZnOH+e^-, \quad (9)$$

$$ZnOH+OH^- \rightarrow Zn(OH)_2^-, \quad (10)$$

$$Zn(OH)_2^-+OH^- \rightarrow Zn(OH)_3^-+e^-, \quad (11)$$

$$Zn(OH)_3^-+OH^- \rightarrow Zn(OH)_4^-+2K^+. \quad (12)$$

Formed active material moves away from the electrode edges and piles up towards the plate bottom and center [10]. The transport of zinc material leads to a reduction of the capacity and serviceable life of the battery (in this work, zinc material refers to all zinc-containing species that involve Zn, ZnO, $Zn(OH)_2$, $K_2Zn(OH)_4$, $Zn(OH)_4^{2-}$, polymeric zinc species, etc.) [11]. Generally, diffusion and convection, as parts of mass transfer, are believed to be too slow to be responsible for the occurrence of electrode shape change. However, it was possible to monitor changes on the electrode/electrolyte interface in the frequency range of 10^{-2}–10^0 Hz of alternating current due formation of the new chemicals with a new dielectric constant (Eq. (1)). Changes in the compounds content and morphology on the electrode surface were detected by scanning electron microscope TESCAN VEGA 3 with BSE imaging (Fig. 5, a–d).

It was found a correlation between the size of Mn and Zn compounds (the size of compounds decreased under high current loads), the distribution of Mn and Zn-contented compounds, the capacitance value, and dispersion in the frequency range of 10^{-2}–100 Hz (Fig. 6). The value of non-Faradaic capacitance has a strong correlation with the content of Zn-species on the surface of the electrode. Increasing the Zn content increased the non-Faradaic capacitance. The dispersion of capacitance also depends on the size of the manganese compounds on the surface in the following sequence: starting sample<10 mA/cm^2< <20 mA/cm^2<30 mA/cm^2~40 mA/cm^2~ ~50 mA/cm^2~60 mA/cm^2.

Analysis of the changes in the capacitance and dispersion of capacitance in the frequency range of 10^{-2}–10^5 Hz detected the most informational range to detect the electrode surface changes. This is the low-frequency range of 10^{-2}–10^1 Hz. Moreover, using three dimensional coordinate systems of the capacitance ratio, the capacitance in low-frequency range dispersion allows us to get a visual picture of the inner changes taking place (Fig. 6,a–f). Also, the changes in the inclination angles of EIS spectrums in Bode coordinates correlate with changing Mn and Zn compounds on the surface.

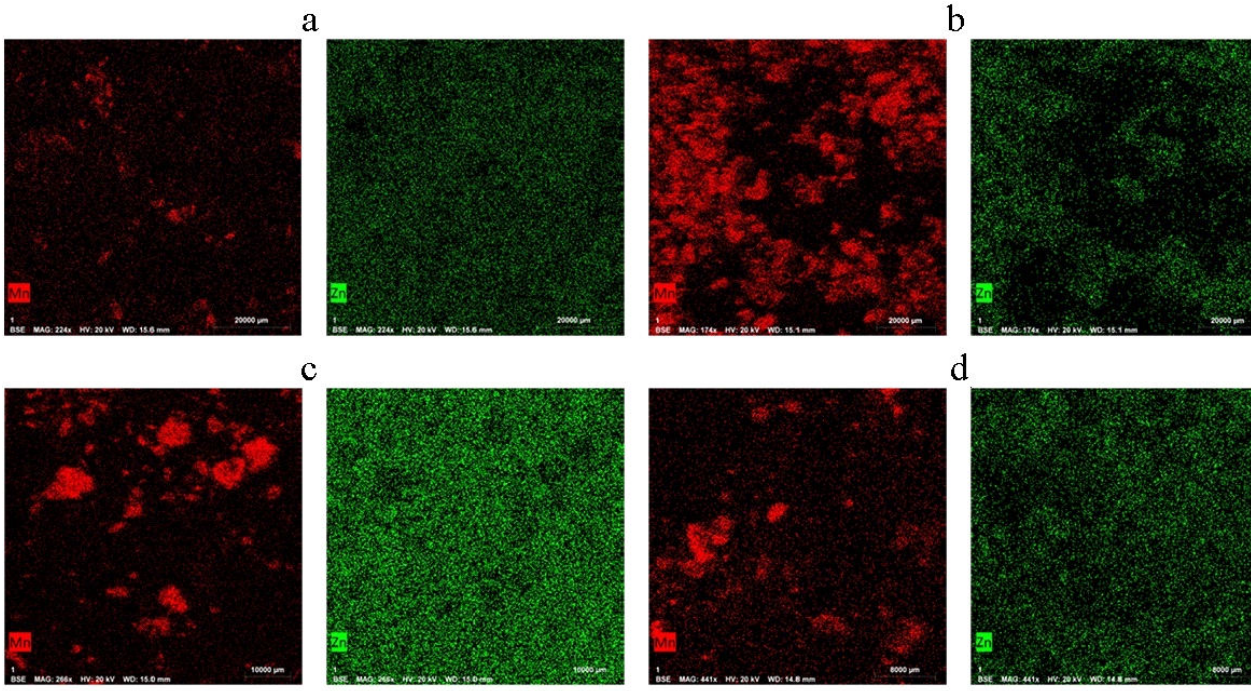

Fig. 5. Surface morphology and distribution of Zn and Mn in the samples before and after current load: (a) starting sample; (b) sample after current load of 10 mA/cm^2; (c) sample after current load of 30 mA/cm^2; (d) sample after current load of 60 mA/cm^2

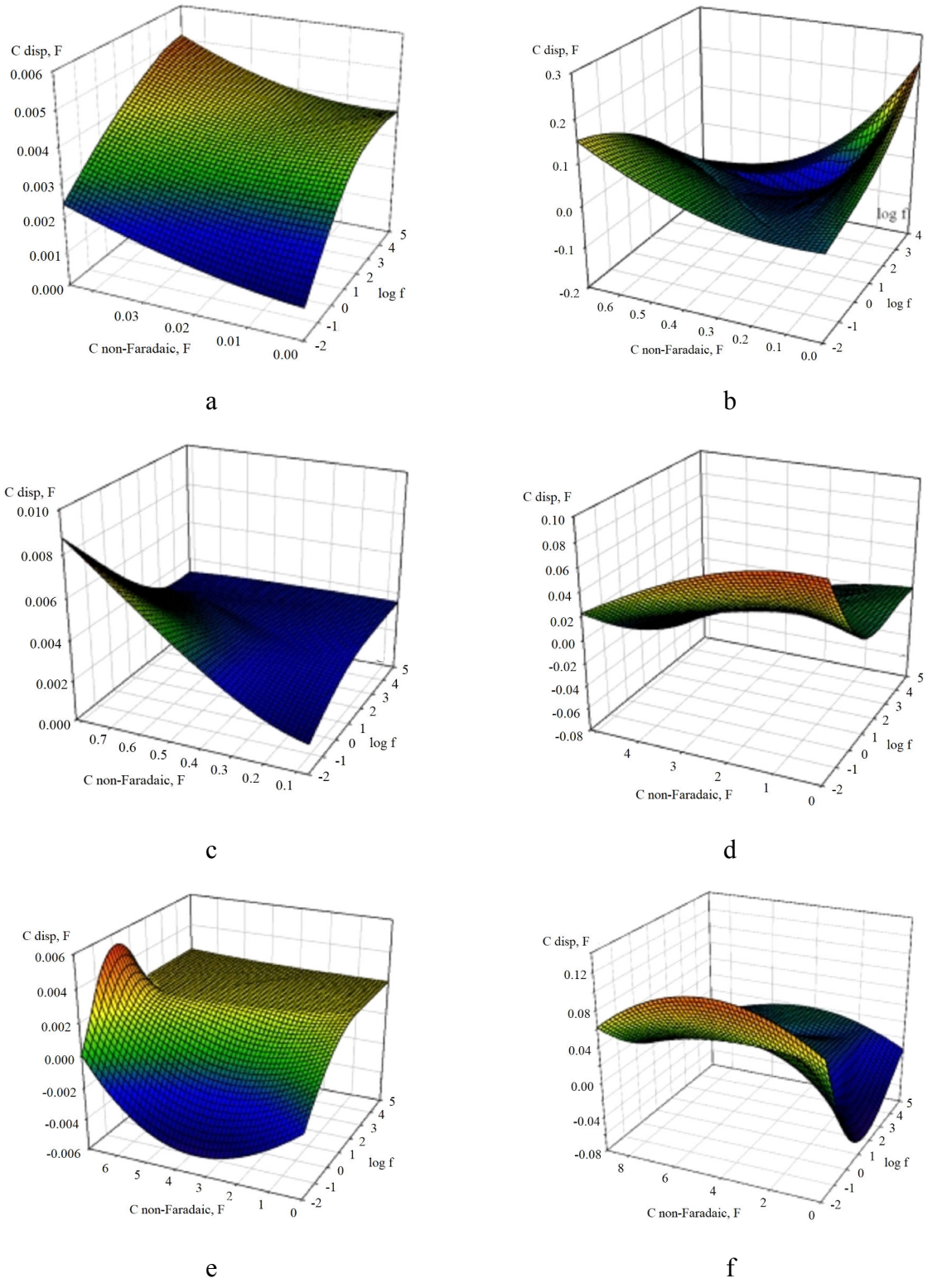

Fig. 6. 3D chart depicting the dispersion of capacitance as a function of non-Faradaic capacitance and frequency at different current loads: (a)10 mA/cm^2; (b) 20 mA/cm^2; (c) 30 mA/cm^2; (d) 40 mA/cm^2; (e) 50 mA/cm^2; and (f) 60 mA/cm^2

Conclusions

A comparative analysis of measurements of changes in electrochemical parameters of primary current sources by the EIS spectroscopy and SEM methods using backscattered electron imaging proved the possibility of practical use of monitoring the operational state of primary current sources. It was experimentally shown that the frequency ranges corresponding to the region of the maximum phase angle shift are the basis for choosing the frequency range for the analysis of the state of the primary current sources. Calculations of capacitance values and their ratios have proven frequency ranges (10^{-2}—100 Hz) that maximally reflect changes on the electrode surface and the degree of electrolyte depletion due to the formation of new manganese and zinc-containing compounds. Using 3D-coordinate systems, the dispersion of capacitance as a function of non-Faradaic capacitance and frequency was constructed that allowed getting a visual picture of the changes taking place. This is manifested in a change in the angles of inclination of the 3D diagrams and an increase in the capacitance values.

Acknowledgments

This work has been supported by the National Academy of Sciences of Ukraine, grant No. 0117U000856. We are grateful to Dr. Stasyk for the help in the SEM study of batteries.

REFERENCES

1. *Chang B.Y., Park S.M.* Electrochemical impedance spectroscopy // Annu. Rev. Anal. Chem. — 2010. — Vol.3. — P.207-229.

2. *Pershina K.D., Kazdobin K.O.* The impedance spectroscopy of the electrolytic materials. — K.: Ukrainian Education, 2012. — 224 p.

3. *Electrochemical* impedance spectroscopy / Wang S., Zhang J., Gharbi O. Vivier V., Gao M., Orazem M.E. // Nat. Rev. Methods Primers. — 2021. — Vol.1. — Art. No. 41.

4. *Lazanas A.C., Prodromidis M.I.* Electrochemical impedance spectroscopy — a tutorial // ACS Meas. Sci. Au. — 2023. — Vol.3. — No. 3. — P.162-193.

5. *Orazem M.E., Tribollet B.* Electrochemical impedance spectroscopy. — New Jersey: John Wiley & Sons, Inc., 2008. — P.383-389.

6. *Electrochemical* impedance spectroscopy for all solid state batteries: theory, methods and future outlook / Vadhva P., Hu J., Johnson M.J., Stocker R., Braglia M., Brett D.J.L., et al. // ChemElectroChem. — 2021. — Vol.8. — No. 11. — P.1930-1947.

7. *Electrochemical* impedance spectroscopy of PEO-LATP model multilayers: ionic charge transport and transfer / Isaac J.A., Mangani L.R., Devaux D., Bouchet R. // ACS Appl. Mater. Interfaces. — 2022. — Vol.14. — No. 11. — P.13158-13168.

8. *Gradient* design of imprinted anode for stable Zn-ion batteries / Cao Q., Gao Y., Pu J., Zhao X., Wang Y., Chen J., et al. // Nat. Commun. — 2023. — Vol.14. — No. 1. — Art. No. 641.

9. *Modeling* insight into battery electrolyte electrochemical stability and interfacial structure / Borodin O., Ren X., Vatamanu J., von Wald Cresce A., Knap J., Xu K. // Acc. Chem. Res. — 2017. — Vol.50. — No. 12. — P.2886-2894.

10. *Riabokin O.L., Bojchuk O.V., Pershina K.D.* The density gradient thermal aging model of the alkaline Zn-Mn batteries // Promising Materials and Processes in Applied Electrochemistry. — 2017. — P.30-34.

11. *Zinc* electrode shape change: II. Process and mechanism / Einerhand R.E.F., Visscher W., De Goeij J.J.M., Barendrecht E. // J. Electrochem. Soc. — 1991. — Vol.138. — No. 1. — P.7-17.

Received 08.05.2024

ПРИКЛАДНІ АСПЕКТИ ВИКОРИСТАННЯ СПЕКТРІВ ІМПЕДАНСУ ДЛЯ КОНТРОЛЮ ПОШКОДЖЕННЯ ЕЛЕКТРОДІВ І ВИСНАЖЕННЯ ЕЛЕКТРОЛІТУ В ПЕРВИННИХ ЦИНК-МАРГАНЦЕВИХ БАТАРЕЯХ

О.Л. Рябокінь, К.Д. Першина

У статті наведено експериментальні та розрахункові дані контролю стану поверхні електрода та виснаження електроліту в первинних Zn-Mn батареях на основі електрохімічної імпедансної спектроскопії та тестів скануючої електронної мікроскопії з використанням зворотно розсіяних електронів. За допомогою цих методів виявлено вплив різних ступенів струмових навантажень на зміну поверхні електродів та їх хімічний склад. Шляхом порівняльного аналізу даних стандартних випробувань і спектрів електрохімічного імпедансу з використанням математичного апарата для змінного струму доведено можливості коректної оцінки робочого стану первинних батарей. Отримані результати можуть бути використані при дослідженнях необоротних змін хімічних джерел і для розвитку теорії пористих електродів.

Ключові слова: цинково-марганцева первинна батарея, нефарадеївська ємність, дисперсія ємності, пошкодження електродів, виснаження електроліту.

APPLIED ASPECTS OF USING ELECTROCHEMICAL IMPEDANCE SPECTROSCOPY SPECTRA FOR MONITORING ELECTRODE DAMAGE AND ELECTROLYTE DEPLETION IN PRIMARY ZINC-MANGANESE BATTERIES

O.L. Riabokin [a], ***K.D. Pershina*** [a, b, *]

[a] **V.I. Vernadsky Institute of General and Inorganic Chemistry, National Academy of Sciences of Ukraine, Kyiv, Ukraine**

[b] **National Technical University of Ukraine «Igor Sikorsky Kyiv Polytechnic Institute», Kyiv, Ukraine**

[*] **e-mail: kathrinepersh@gmail.com**

The article presents experimental and computational data on monitoring electrode surface condition and electrolyte depletion in primary Zn-Mn batteries using electrochemical impedance spectroscopy and scanning electron microscopy with backscattered electrons. These methods reveal the impact of different current load levels on changes in electrode surfaces and their chemical composition. Through comparative analysis of data from standard tests and electrochemical impedance spectroscopy spectra using mathematical tools for alternating current analysis, the feasibility of accurately assessing the operational state of primary batteries is demonstrated. The results obtained can be applied to studies of irreversible changes in chemical power sources and to the development of the theory of porous electrodes.

Keywords: zinc-manganese primary battery; non-Faradaic capacitance; capacity dispersion; electrode damage; electrolyte depletion.

REFERENCES

1. Chang BY, Park SM. Electrochemical impedance spectroscopy. *Annu Rev Anal Chem*. 2010; 3: 207-229. doi: 10.1146/annurev.anchem.012809.102211.

2. Pershina KD, Kazdobin KO. *The impedance spectroscopy of the electrolytic materials*. Kyiv: Ukrainian Education; 2012. 224 p. (*in Ukrainian*).

3. Wang S, Zhang J, Gharbi O, Vivier V, Gao M, Orazem ME. Electrochemical impedance spectroscopy. *Nat Rev Methods Primers*. 2021; 1: 41. doi: 10.1038/s43586-021-00039-w.

4. Lazanas AC, Prodromidis MI. Electrochemical impedance spectroscopy – a tutorial. *ACS Meas Sci Au*. 2023; 3(3): 162-193. doi: 10.1021/acsmeasuresciau.2c00070.

5. Orazem ME, Tribollet B. *Electrochemical impedance spectroscopy*. John Wiley & Sons, Inc; 2008. doi: 10.1002/9780470381588.

6. Vadhva P, Hu J, Johnson MJ, Stocker R, Braglia M, Brett DJL, et al. Electrochemical impedance spectroscopy for all-solid-state batteries: theory, methods and future outlook. *ChemElectroChem*. 2021; 8: 1930-1947. doi: 10.1002/celc.202100108.

7. Isaac JA, Mangani LR, Devaux D, Bouchet R. Electrochemical impedance spectroscopy of PEO-LATP model multilayers: ionic charge transport and transfer. *ACS Appl Materials Interfaces*. 2022; 14(11): 13158-13168. doi: 10.1021/acsami.1c19235.

8. Cao Q, Gao Y, Pu J, Zhao X, Wang Y, Chen J, et al. Gradient design of imprinted anode for stable Zn-ion batteries. *Nat Commun*. 2023; 14(1): 641. doi: 10.1038/s41467-023-36386-3.

9. Borodin O, Ren X, Vatamanu J, von Wald Cresce A, Knap J, Xu K. Modeling insight into battery electrolyte electrochemical stability and interfacial structure. *Acc Chem Res*. 2017; 50(12): 2886-2894. doi: 10.1021/acs.accounts.7b00486.

10. Riabokin OL, Bojchuk OV, Pershina KD. The density gradient thermal aging model of the alkaline Zn-Mn batteries. *Promising Materials and Processes in Applied Electrochemistry*. 2017; 30-34.

11. Einerhand REF, Visscher W, De Goeij JJM, Barendrecht E. Zinc electrode shape change: II. Process and mechanism. *J Electrochem Soc*. 1991; 138(1): 7-17. doi: 10.1149/1.2085582.